PHYSICAL REVIEW B **72**, 081309(R) (2005)

Localized high-energy emissions from the vicinity of defects in high-efficiency $Ga_xIn_{1-x}N/GaN$ quantum wells

F. Hitzel,* G. Klewer, S. Lahmann, U. Rossow, and A. Hangleiter†

Institute of Applied Physics, Technical University of Braunschweig, Mendelssohnstrasse 2, D-38106 Braunschweig, Germany

(Received 23 March 2005; revised manuscript received 24 June 2005; published 23 August 2005)

Using a high-resolution low-temperature spectroscopic scanning near-field optical microscope we observe highly localized high-energy emissions from highly efficient $Ga_xIn_{1-x}N/GaN$ quantum wells. These sharp emissions about 300–400 meV above the main quantum well luminescence are characteristic for high-efficiency structures and originate from the immediate vicinity of threading dislocations. Thus, areas of increased bandgap surrounding the defects appear to exist only in high-efficiency structures, which act as barriers prohibiting carriers from recombining nonradiatively at the defects.

DOI: 10.1103/PhysRevB.72.081309 PACS number(s): 78.67.De, 77.84.Bw, 61.72.Lk, 73.21.Fg

Quantum wells (QW's) based on $Ga_xIn_{1-x}N/GaN$ heterostructures emitting in the visible and near ultraviolet spectral range exhibit an astoundingly large light emission efficiency even when based on heteroepitaxial structures with a large density of threading dislocations[1] of up to 10^{10} cm^{-2}. On the other hand, similar In-free structures for the ultraviolet based on GaN/AlGaN show much lower emission efficiency. It is now quite common to attribute the unusual efficiency of the GaInN-based structures to extremely strong carrier localization due to compositional fluctuations[2] or even phase separation in the GaInN,[3] which is thought to prevent carriers from reaching the defects and from recombining nonradiatively.[4]

The optical properties of such QW's are strongly influenced by the strong lattice mismatch between GaInN and GaN (or between GaN and AlGaN) and the resulting pseudomorphic strain field in the highly polar lattice, which leads to a strong piezoelectric polarization[5,6] inside the quantum wells. The huge internal field (of the order MV/cm)[7] in turn gives rise to a strong "quantum confined Stark effect" (QCSE) first observed in GaAs-based quantum wells.[8] In addition to a strong redshift of the emission,[5] a dramatic reduction of the oscillator strength may thus result from these fields.[6,9] In fact, most of the unusual optical properties of nitride quantum wells may be well understood on the basis of the polarization fields.[10] However, the internal fields provide no explanation of the unusually large emission efficiency of such structures. On the contrary, one might expect an even smaller efficiency due to the reduced oscillator strength.[6]

In addition, the optical properties may be affected by compositional fluctuations,[2] if present. These fluctuations contribute to the large emission linewidth[11] as well as to a large "Stokes-like" shift of the emission relative to the absorption edge.[2,11]

We have used high-resolution low-temperature near-field microscopy to collect local emission spectra from high-efficiency $Ga_xIn_{1-x}N/GaN$ quantum wells in order to clarify the reasons for their unexpected behavior. Our results show that the emission distribution is correlated to the defect structure and that localized emissions at higher energy coming from the vicinity of defects indicate regions of larger bandgap.

Our samples were grown on *c*-plane sapphire substrates using low-pressure metal-organic vapor phase epitaxy in a horizontal reactor (AIX 200RF). Trimethylgallium, triethylgallium, trimethylindium, and trimethylaluminum were used as group-III sources, and ammonia was used as group-V source. Typical structures consist of a GaN nucleation layer grown at 560 °C, a 1.8 μm thick GaN buffer layer grown at 1180 °C, a single or double quantum well region with 2–3 nm wells and 8 nm barriers grown at 835 °C (total pressure 200 mbar, total flux 4.5 slpm, ammonia flow 2000 sccm, carrier gas N_2), an AlGaN electron barrier layer of about 10 nm, and a 130 nm GaN capping layer. All structures reported here were nominally undoped. The thicknesses and growth rates in the active region were determined by high-resolution x-ray diffraction and confirmed by transmission electron microscopy.

The samples were investigated using a low-temperature scanning near-field optical microscope (SNOM) attached to a spectrometer equipped with a liquid-nitrogen cooled charge-coupled-device (CCD) detector, running in illumination-collection mode. The SNOM can be operated both at low temperature (20 K) or at room temperature. Fiber probes were homemade using a tube-etching process and metal coated with aluminum. Optical excitation during SNOM measurements was performed using the 335 nm line of an Ar-ion laser. Typical SNOM measurements consist of scanning 128×128 points on a 5×5 μm area, collecting a complete emission spectrum at each point. The spatial resolution obtained with our instrument was better than $\lambda/10$ under optimum conditions, the spectral resolution was set to about 1.5 nm

The internal quantum efficiency of our samples is routinely determined using temperature and excitation power dependent photoluminescence measurements based on resonant excitation with the 380 nm line of the Ar-ion laser. Details of the procedure are described in Ref. 12. The optimization of the growth procedure was guided by the results of such measurements.

In the following we will specifically discuss data obtained for two samples, which have similar emission wavelengths of 430 nm (sample A, double QW) and 440 nm (sample B, single QW) but differ strongly in their room temperature

 ©2005 The American Physical Society

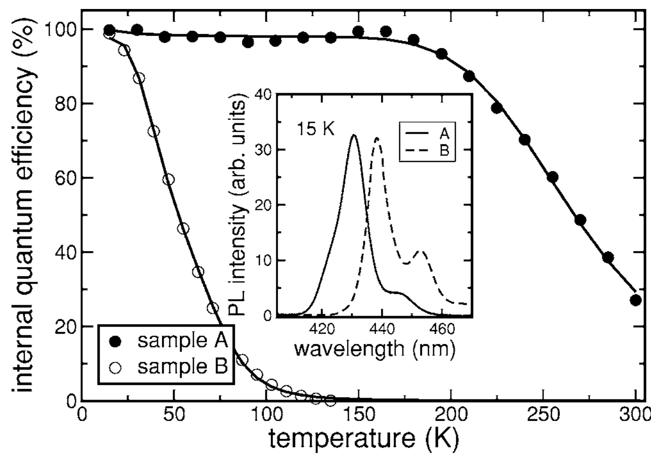

FIG. 1. Temperature-dependent internal quantum efficiency of two typical samples investigated. The inset shows low-temperature photoluminescence spectra.

(RT) internal quantum efficiency. As shown in Fig. 1, sample A reaches an internal efficiency of about 30% at RT, while sample B hardly emits any light at RT, i.e. has a quantum efficiency below 10^{-3}. Still, the two samples exhibit quite comparable photoluminescence intensities at low temperature.

Looking at the two samples with the SNOM and focusing on the spectrally integrated low-temperature (20 K) emission intensity as in Fig. 2, we note that strong local intensity variations occur in both samples. The characteristic length scale of the intensity variations is of the order a few hundred nanometers in both cases. The typical density of threading dislocations is about 10^9 cm^{-2} in these samples, i.e. the typical average distance of dislocations is about 300 nm. Sample C in Fig. 2 has dislocations decorated and was imaged using a dedicated atomic force microscope (AFM). The AFM image shows that the observed intensity pattern in the SNOM images is obviously correlated with the dislocation structure. Unfortunately, the topography information available from the near-field microscope does not allow us to resolve the position of single dislocations.

Nevertheless, as far as the spectrally integrated intensity distribution is concerned, we may conclude that the two samples exhibit a similar behavior.

The situation becomes different when looking at single-wavelength images, also taken at low temperature. While such images taken at wavelengths close to the peak of the main QW emission are very similar to the integrated images shown in Fig. 2, images for wavelengths in the range 380–410 nm taken for sample A are vastly different: Nanometer-sized bright spots appear which change quickly at different wavelengths. Figure 3(a) shows three such images at wavelengths of 385 nm, 400 nm, and 409 nm combined using a color-coding scheme. Pure red, green, or blue spots in this image indicate dominant emission at one particular wavelength from this spot. Mixed colors (additive color mixing) indicate contributions from several wavelengths. The typical diameter of those spots is of the order 100–200 nm, most likely limited by the resolution of the near-field probe used in this measurement.

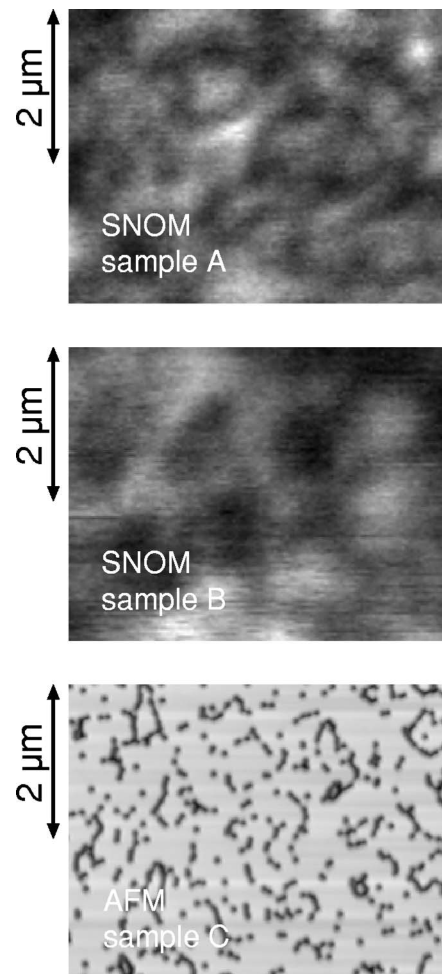

FIG. 2. Spectrally integrated low-temperature near-field images of samples A and B covering a 5×3.8 μm area with 128×98 scan points. The grey value represents the emission intensity. An AFM image of a (different) sample C with dislocations marked shows the typical dislocation structure. The spatial structure of both images reflects the distribution of threading dislocations.

In Fig. 3(b) we show local spectra, each taken at one of the respective bright spots and plotted using the same color coding. We observe narrow emission lines, with spectral widths down to 2 nm, in addition to the main QW emission at 430 nm. The local spectra are an individual fingerprint of each of the bright spots in Fig. 3(a), which show that additional emissions occur in the wavelength range 380–410 nm. Each of the local spectra exhibiting the short-wavelength emissions also shows a contribution of the main 430 nm emission, although at much lower intensity compared to areas where the main emission is bright. This is a likely consequence of the finite spatial resolution, which mixes emissions from areas emitting at short-wavelength and those emitting at the main 430 nm peak.

All attempts to find similar short-wavelength emissions from sample B produced negative results: For sample B we find no structure in the near-field images taken at wavelengths shorter than the main emission. Given our sensitivity and noise level we can say that short-wavelength contributions from sample B are at least one order of magnitude

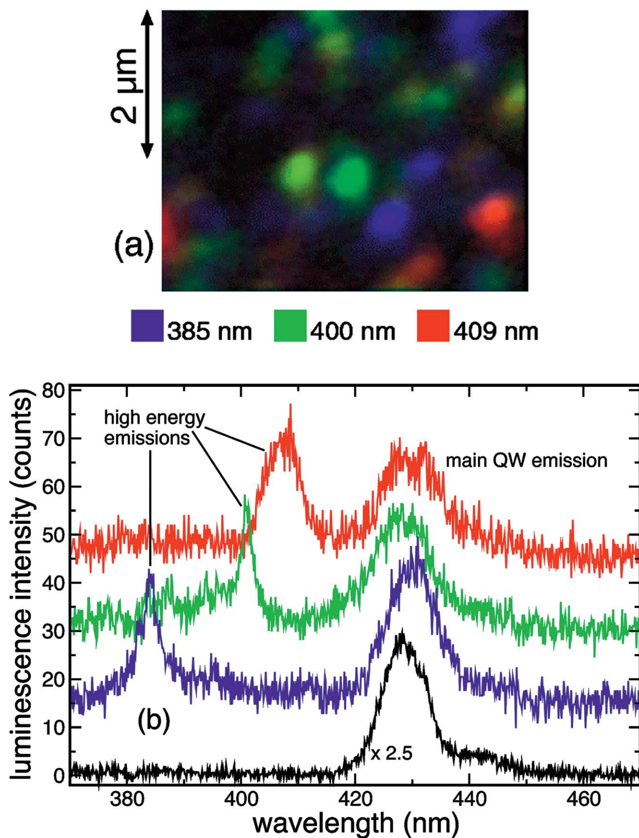

FIG. 3. (Color) Combined near-field image of selected emissions at short wavelength (a) and corresponding local spectra (b) from sample A. As the signal from regions emitting at the main 430 nm line (lowest spectrum) is much stronger than the short-wavelength emission, there is always some crosstalk of the 430 nm emission. The colors in the near-field image represent contributions at different wavelengths, the brightness of the colors represents their intensity.

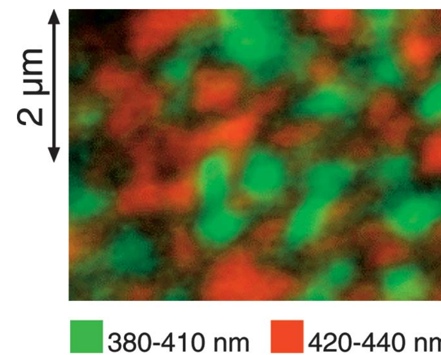

FIG. 4. (Color) Combined near-field image of the integrated short-wavelength range (green) and the long-wavelength range (red). The brightness of the colors repesents the emission intensity. True complementarity is observed.

weaker than those observed from sample A. On the other hand, other high-efficiency samples like sample A always exhibited such short-wavelength emissions, not all of which are as bright as observed for sample A discussed here.

In order to understand the origin of the short-wavelength, high-energy emissions we take two images, one integrating the short-wavelength part of the spectra (380–410 nm), the other integrating the longer-wavelength part of the spectra (420–440 nm). In Fig. 4 we again use a color-coding procedure, where the longer-wavelength image is in red and the shorter-wavelength image is in green, both combined using additive color mixing.

Most importantly, we note that the two contributions are truly complementary, i.e. regions strongly emitting at the main 430 nm line are dim in the short-wavelength image and vice versa. This is immediately visible from the lack of yellowish regions in Fig. 4, as a mixture of of red and green would produce yellow. This means that regions emitting at high energy do not significantly contribute to the main emission.

Moreover, we also see from Fig. 4 that there are essentially no dark regions, i.e. at any position in the image area there is either emission on the main 430 nm line or in the high-energy range. One would expect defects to produce dark areas for the main emission, but obviously all those areas dark in the main emission do emit in the high-energy range. Thus we must conclude that the high-energy emissions come from regions close to the defects. If in turn all regions close to defects emit at higher energy, those regions must have a higher bandgap than the normal quantum wells “far” from the defects.

Based on these observations, an interesting picture explaining the high emission efficiency of such samples emerges: If defects are surrounded by regions exhibiting a bandgap larger than that of the “normal” QW’s, then carriers at energies around the “normal” bandgap (i.e. 430 nm in the present case) need to overcome an energy barrier in order to move towards the defects and to recombine nonradiatively. If the difference in bandgap is large enough (300–400 meV in the present case) the thermal energy of carriers even at room temperature will not be sufficient to allow them reaching the defects.

It is interesting to consider the possible origin of the high-bandgap regions. In quantum well structures, a larger bandgap can be the consequence of (i) reduced In incorporation, (ii) reduced well width, or (iii) reduced strain or polarization field. For the high-efficiency samples investigated in this study, it seems that one of these mechanisms takes place in the vicinity of threading dislocations. In fact, Duxbury *et al.*[13] have observed reduced In content close to dislocations in GaInN multiple quantum wells.

On the other hand, no evidence for high-bandgap regions was found for low-efficiency samples. Rather than that, dark areas with no emission are observed for such samples. As the nucleation and buffer layers of the samples are nominally identical, very similar defect densities are expected. Thus we conclude that in case of low-efficiency samples, no high-bandgap regions are generated during growth such that dislocations remain active recombination centers.

For the two specific samples discussed here, it appears that the double QW exhibits high efficiency along with high-energy emissions, while the single QW shows low efficiency and no high-energy emissions. Such a difference in efficiency is observed for several other similar single and double

QW samples. One may speculate that growth of a quantum well on top of another one leads to conditions favorable for high emission efficiency.

The existence of high-bandgap regions surrounding the defects may represent an alternative mechanism for high efficiency, contrasting with the usual localization picture. In fact, if more or less all the defects are decorated with such barriers, even mobile free excitons may become immune to nonradiative recombination.

In conclusion, we have compared high and low-efficiency $Ga_xIn_{1-x}N/GaN$ quantum wells using spectroscopic near-field microscopy. Only for high-efficiency samples we find emissions at higher energy originating from the vicinity of defects. The higher bandgap regions associated with the high-energy emissions are likely to represent barriers surrounding the defects, which prohibit nonradiative recombination.

Partial financial support of this work by the Deutsche Forschungsgemeinschaft is gratefully acknowledged.

---

*Present address: Danish Micro Engineering A/S, Transformervej 12, DK-2730 Herlev, Denmark.

†Electronic address: a.hangleiter@tu-bs.de

[1] S. D. Lester, F. A. Ponce, M. G. Craford, and D. A. Steigerwald, Appl. Phys. Lett. **66**, 1249 (1995).

[2] S. Chichibu, T. Azuhata, T. Sota, and S. Nakamura, Appl. Phys. Lett. **69**, 4188 (1996).

[3] Y. Narukawa, Y. Kawakami, M. Funato, S. Fujita, S. Fujita, and S. Nakamura, Appl. Phys. Lett. **70**, 981 (1997).

[4] S. Nakamura, Science **281**, 956 (1998).

[5] T. Takeuchi, S. Sota, M. Katsuragawa, M. Komori, H. Takeuchi, H. Amano, and I. Akasaki, Jpn. J. Appl. Phys. **36**, L382 (1997).

[6] J. S. Im, H. Kollmer, J. Off, A. Sohmer, F. Scholz, and A. Hangleiter, Phys. Rev. B **57**, R9435 (1998).

[7] A. Hangleiter, F. Hitzel, S. Lahmann, and U. Rossow, Appl. Phys. Lett. **83**, 1169 (2003).

[8] E. E. Mendez, G. Bastard, L. L. Chang, L. Esaki, H. Morkoc, and R. Fischer, Phys. Rev. B **26**, 7101 (1982).

[9] A. Hangleiter, J. S. Im, H. Kollmer, S. Heppel, J. Off, and F. Scholz, MRS Internet J. Nitride Semicond. Res. **3**, 15 (1998).

[10] A. Hangleiter, *Low-Dimensional Nitride Semiconductors*, edited by B. Gil (Oxford University Press, New York, 2002), Chap. 13.

[11] A. Hangleiter, J. S. Im, J. Off, and F. Scholz, Phys. Status Solidi B **216**, 427 (1999).

[12] A. Hangleiter, D. Fuhrmann, M. Grewe, F. Hitzel, G. Klewer, S. Lahmann, C. Netzel, N. Riedel, and U. Rossow, Phys. Status Solidi A **201**, 2808 (2004).

[13] N. Duxbury, U. Bangert, P. Dawson, E. J. Thrush, W. V. der Stricht, K. Jacobs, and I. Moerman, Appl. Phys. Lett. **76**, 1600 (2000).